# Accumulated-Energy-Controlled Nanosecond UV Laser Microvia Drilling In Cu–PI Copper-Clad Laminates

Duong Duc Tai[1,2] and Vu Van Quang[1*]

[1] Precision Engineering & Smart Measurement Lab, School of Mechanical Engineering, Hanoi University of Science and Technology, No. 1 Dai Co Viet Street, Hanoi 100000, Vietnam.
[2] Sumitomo Electronic Components (Vietnam) Co., Ltd
[*] Corresponding author. E-mail: quang.vuvan1@hust.edu.vn

Received: Jun. 20, 2026; Accepted: Aug. 03, 2026

Conductive microvias in flexible printed circuits (FPCs) play a critical role in establishing electrical interconnections between circuit layers and directly affect the reliability of electronic systems. However, microvia drilling in flexible copper-clad laminate (FCCL) substrates with heterogeneous Cu-PI structures remain challenging because copper and polyimide exhibit significantly different optical, thermal, and ablation characteristics. This study proposes an integrated nanosecond UV laser machining strategy in which laser power, pulse repetition rate, scanning speed, and pressure-assisted debris extraction are coordinated to control the accumulated energy distribution and improve microvia quality. The hole-formation and material-removal mechanisms are analyzed based on laser–material interaction theory and an accumulated-energy model to guide parameter selection. Experiments were conducted using an industrial 355 nm UV Nd:YAG laser system with spiral and circular drilling strategies. The results show that the optimized processing conditions, combining lower laser power, lower pulse repetition rate, higher scanning speed, and pressure-assisted debris removal, improved the taper ratio by 18.94 percentage points for spiral drilling and 6.42 percentage points for circular drilling compared with the baseline conditions. EDX analysis indicated a reduction in carbon-containing residues on the microvia sidewalls, with the carbon content decreasing from 11.87% to 9.29% for spiral drilling and from 8.86% to 7.54% for circular drilling. Meanwhile, SEM observations and laser microscopy confirmed improvements in hole geometry, surface quality, and taper control. These findings demonstrate the potential of the proposed strategy for stable and industrially compatible microvia fabrication in flexible electronic circuits.

**Keywords:** Conductive microvias; Flexible printed circuits/ FPCs; Nanosecond UV laser machining; microvia quality; Cu-PI structures.

©The Author('s). This is an open-access article distributed under the terms of the Creative Commons Attribution License (CC BY 4.0), which permits unrestricted use, distribution, and reproduction in any medium, provided the original author and source are cited.

http://dx.doi.org/10.6180/jase.202612_35.022

## 1. Introduction

Flexible printed circuits (FPCs) and flexible copper-clad laminates (FCCLs) are essential components of high-density electronic systems because of their low weight, mechanical flexibility, and compatibility with advanced packaging technologies. In multilayer structures, microvias provide vertical electrical interconnections and directly influence circuit reliability. However, laser drilling of microvias remains challenging because copper and polymer exhibit substantially different optical, thermal, and ablation characteristics [1–3].

Short and ultrashort-pulse lasers are widely used for microvia and microhole fabrication because they enable non-contact material removal, high positioning accuracy, and flexible process control. Microvia geometry and surface quality are strongly affected by pulse energy, pulse-repetition rate, focal position, scanning speed, and pulse overlap. Inadequate control of these parameters may lead to excessive taper, recast-layer formation, material redeposition, and microcracking [4–7].

Scanning trajectories strongly influence accumulated-energy distribution, material-removal behavior, hole circularity, taper, sidewall morphology, and debris evacuation. Spiral and helical trajectories facilitate progressive material removal and provide greater geometric control during microhole drilling [8, 9], whereas dual-path scanning, beam-track modulation, beam-incidence control, annular drilling, and trepanning have been investigated to further control hole morphology and taper [10–14]. However, the direct application of these strategies to heterogeneous CCL and FCCL structures remains challenging because copper and polymer respond differently to laser irradiation. In addition, the Gaussian intensity distribution of the laser beam and non-uniform pulse overlap during high-speed scanning may cause localized energy accumulation, non-uniform ablation, and variations in microvia geometry [1, 2, 5–7].

Previous studies on metallic alloys, coated superalloys, and copper have investigated high-aspect-ratio drilling, parameter optimization, breakthrough control, material-removal behavior, and surface integrity, demonstrating the strong dependence of microhole quality on laser parameters and pulse accumulation [15–19]. More advanced approaches, including burst-mode processing and spatial or temporal beam shaping, have also been developed to improve machining efficiency and geometric control [20–22]. In addition, static or flowing-water assistance, complex water-assisted drilling, and wet-assisted processing have been investigated to suppress thermal damage and improve microhole quality [23–26]. Backside water assistance, multi-energy-field-assisted processing, water-assisted layered drilling, and solution- or mist-assisted methods have further demonstrated the potential of auxiliary media for improving debris evacuation and reducing machining defects [27–30]. However, these approaches may require specialized laser operating modes, additional optical configurations, post-processing steps, or auxiliary liquid-handling systems, thereby-increasing process complexity and limiting their direct integration into high-throughput dry manufacturing lines for flexible electronics.

Despite these advances, several research gaps remain. A substantial proportion of previous laser micro drilling studies have focused on homogeneous metals, superalloys, ceramics, and coated engineering materials, whereas systematic investigations of microvia formation in heterogeneous copper-polymer structures remain relatively limited [1, 2, 15–19]. Furthermore, laser parameters, scanning trajectories, and material-removal behavior are frequently investigated as individual factors, although practical CCL and FCCL processing is governed by their coupled effects on pulse accumulation, scanning dynamics, thermal relaxation, and debris evacuation [5–9, 19]. Therefore, an integrated process-control strategy is required to improve microvia quality without substantially increasing the complexity of the optical and manufacturing systems.

To address these limitations, this study proposes a physics-guided process-control framework that integrates average laser power, pulse-repetition rate, scanning speed, galvanometer motion, accumulated-energy distribution, and dry vacuum-assisted debris extraction into a unified parameter-selection strategy. Although $CO_2$ lasers have been widely applied to the processing of polymer-based composite materials [31], shorter-wavelength UV irradiation provides important advantages in beam focusing and localized material interaction for the high-precision machining of heterogeneous copper-polymer structures. Therefore, a 355 nm UV Nd laser was selected because it enables effective micromachining of copper, a smaller focused spot, and a more localized processing region, while UV laser systems have also demonstrated practical applicability to flexible PCB drilling [3, 32, 33]. These characteristics make 355 nm UV irradiation suitable for high-precision microvia machining of CCL and FCCL structures.

The proposed process was designed to achieve a taper ratio of at least 85% while maintaining both the entrance and bottom diameters within $\pm5\%$ of their nominal values. Sidewall integrity, residual debris, recast-layer formation, and residual carbon content below 15% were additionally adopted as complementary criteria for evaluating process feasibility and compatibility with subsequent metallization.

Unlike conventional approaches that increase laser power or pulse overlap to enhance material removal, the proposed strategy coordinates lower average laser power and pulse-repetition rate with higher scanning speed. A lower pulse-repetition rate increases the interval between successive pulses and allows partial thermal relaxation of the irradiated region, whereas a higher scanning speed reduces excessive local pulse accumulation. The coordinated adjustment of these parameters promotes a more controlled accumulated-energy distribution despite the Gaussian beam profile, thereby reducing localized overheating, non-uniform ablation, and excessive taper formation. A dry vacuum-assisted debris-extraction mechanism is further incorporated to facilitate debris removal and suppress material redeposition during microvia drilling.

The novelty of this study lies in the development and experimental validation of an integrated process-control strategy that combines accumulated-energy control, galvanometer-scanning dynamics, and dry vacuum-assisted debris extraction to coordinate average laser power, pulse-repetition rate, and scanning speed, rather than optimizing individual parameters through trial-and-error experimentation. Compared with approaches requiring femtosecond or picosecond laser sources, beam-shaping modules, specialized pulse modes, or liquid-assisted processing environments, the proposed strategy can be implemented mainly by adjusting parameters already available on an industrial nanosecond UV laser platform without replacing the laser source or substantially modifying the core optical architecture. The use of dry vacuum-assisted debris extraction also avoids the need for additional liquid supply, recovery, drying, and treatment systems. Therefore, the proposed approach provides methodological novelty through integrated process control while reducing system complexity and additional capital investment, thereby facilitating implementation in large-scale dry FPC manufacturing lines.

The proposed strategy was experimentally validated using an industrial nanosecond UV laser system employed for FPC manufacturing in Vietnam. Representative processing parameters and results are reported while preserving industrial confidentiality. Microvia quality was evaluated in terms of dimensional accuracy, taper ratio, sidewall morphology, residual debris, and elemental composition using optical measurements, scanning electron microscopy, and energy-dispersive X-ray spectroscopy. The results demonstrate the practical feasibility of the proposed integrated process-control strategy for improving microvia quality under industrial manufacturing conditions.

## 2. Theory and formula

To effectively control laser material ablation, the workpiece surface must be maintained within the effective focal region of the beam, commonly characterized by the depth of focus and related to the Rayleigh length of the optical system [34]. Beam focusing is required to achieve the fluence necessary to exceed the ablation threshold while controlling the focal spot size and thermal influence on the material. If the focal position is unstable, the surface fluence may vary, leading to deviations in hole geometry, enlargement of the heat-affected region, and deterioration of machining quality [35, 36].

In a Galvo F-theta system, the F-theta lens is used to generate an approximately flat focal field over the scanning area, helping to maintain a relatively stable spot size and energy distribution within the designed working range. However, variations in scanning angle may still induce focal shift or spot distortion if the optical system is not properly aligned or compensated [37, 38]. Therefore, controlling the focal position and beam characteristics is essential for ensuring repeatable microvia machining.

Laser-material interaction is commonly described using a Gaussian intensity distribution, where the fluence is highest at the beam center and decreases radially. This distribution determines the region in which the material exceeds the ablation threshold, thereby affecting the entrance diameter, taper angle, drilling depth, and heat-affected zone [39]. In nanosecond pulsed UV laser machining, microvia quality depends not only on single-pulse energy but also on pulse accumulation density, pulse overlap, scanning speed, and the thermal relaxation interval between consecutive pulses.

However, the ideal Gaussian model does not fully capture the dynamic changes occurring during drilling. Continuous material removal can generate microstructures, resolidified layers, secondary channels, and redeposited debris within the machined region [40]. These features alter laser absorption, reflection, and scattering, particularly in heterogeneous CCL/FCCL substrates composed of copper and polymer layers. Therefore, effective ablation control should simultaneously consider focal positioning, Gaussian energy distribution, pulse accumulation, galvanometer scanning dynamics, and debris removal behavior.

Laser material ablation is initiated when the material surface absorbs optical energy and the local energy density exceeds the ablation threshold of the material [41]. The ablation efficiency depends on the conversion of the instantaneous laser power density $I(t,r)$ into absorbed energy during the pulse-material interaction. For a single laser pulse $i^{\text{th}}$ with center position $r_i$, the pulse width $\tau$ is regarded as the effective interaction time. Therefore, the accumulated energy density at a radial position $r$ on the workpiece surface can be obtained by integrating the instantaneous power density over the pulse duration:

$$Q_i(r) = \int_0^r I_i(t,r)dt \tag{1}$$

where $Q_i(r)$ is the single-pulse energy density. Material ablation can be initiated when $Q_i(r)$ exceeds the ablation threshold $Q_{th}$. Based on the Gaussian beam assumption and the power conservation condition, the instantaneous power density can be expressed as:

$$I_i(t,r) = \frac{8P_{\text{avg}}}{\pi f t\sqrt{\pi}d^2}\exp\left(\frac{-t^2}{\tau^2}\right)\exp\left(\frac{-8\left(r-r_i\right)^2}{d^2}\right) \tag{2}$$

where $P_{\text{avg}}$ is the average laser power, $f$ is the pulse repetition rate, $\tau$ is the pulse width, and $d$ is the laser spot diameter at the machining plane. The quantity $I_i(t,r)$, expressed in $W/m^2$, represents the instantaneous power density at radial position $r$ and time $t$. By integrating $I_i(t,r)$ from 0 to $r$, the single-pulse energy density can be written as:

$$Q_i(r) = \frac{4P_{avg}}{\pi f d^2} \exp\left(\frac{-8\,(r-r_i)^2}{d^2}\right) \tag{3}$$

For stable ablation, the accumulated energy density should exceed the ablation threshold while remaining within an appropriate processing window to avoid excessive ablation and thermal degradation. In short-pulse laser machining, stable material removal is generally not governed by a single pulse alone, but by the accumulated energy delivered by multiple successive pulses within the machining region. Since the exact beam-center position of each pulse during high-speed galvanometer scanning is difficult to determine, a simplified effective accumulation model is adopted. In this model, the contribution of successive pulses is represented by an effective pulse number $n_{\text{eff}}$ , rather than by tracking the individual position of each pulse. Thus, the accumulated energy density at position $r$ can be approximated as:

$$\begin{aligned} Q_{acc}(r) &\approx \sum_i Q_i(r) \approx \sum_{i=0}^{n_{\text{eff}}} \frac{4P_{\text{avg}}\cdot \text{erf}(1)}{\pi f d^2} \exp\left(\frac{-8\,(r-r_i)^2}{d^2}\right) \\ Q_{\text{acc}}(r) &\approx \frac{1.073P_{\text{avg}}}{f d^2} \sum_{i=0}^{n_{\text{eff}}} \exp\left(\frac{-8\,(r-r_i)^2}{d^2}\right) \end{aligned} \tag{4}$$

At positions away from the beam center, where $r$ increases toward the edge of the laser spot, the energy density decreases according to the Gaussian distribution. This radial decay leads to non-uniform material removal, causing differences between the entrance and bottom diameters and producing taper or profile deviation. Regions receiving higher accumulated energy tend to generate greater drilling depth, whereas regions receiving insufficient energy may be only partially ablated. Therefore, improving the spatial uniformity of $Q_{\text{acc}}(r)$ is essential for controlling microvia geometry, taper angle, and surface quality [42, 43].

Based on this model, the proposed strategy does not rely simply on increasing laser power or pulse energy. Instead, the process parameters are coordinated to redistribute the accumulated fluence within the machining region. The average power is reduced to limit excessive peak energy at the beam center, while the repetition rate and scanning speed are adjusted to control the effective pulse number and pulse overlap. Decreasing the repetition rate increases the temporal interval between successive pulses, allowing partial thermal relaxation, whereas increasing the scanning speed enlarges the spatial separation between adjacent pulses and suppresses excessive local overlap. Through this coordinated control, the accumulated fluence can be maintained above the ablation threshold while reducing localized energy concentration and thermal accumulation.

For heterogeneous Cu-PI CCL/FCCL substrates, this control is especially important because copper and polymer layers exhibit different optical absorption, thermal conductivity, and ablation thresholds. Therefore, a processing condition that is suitable for one layer may cause insufficient removal or excessive thermal damage in the other. To improve process stability, the energy distribution model is used to guide the selection of average power, repetition rate, scanning speed, and machining time for individual microvias. In addition, a pressure differential driven extraction mechanism is integrated to remove ablated debris from the machining zone. This mechanism reduces beam shielding, remelting, and redeposition of debris under subsequent laser pulses, thereby minimizing recast-layer formation and improving the final surface quality.

Based on mathematical formulation, a graphical model is established to quantitatively determine the accumulated fluence distribution.

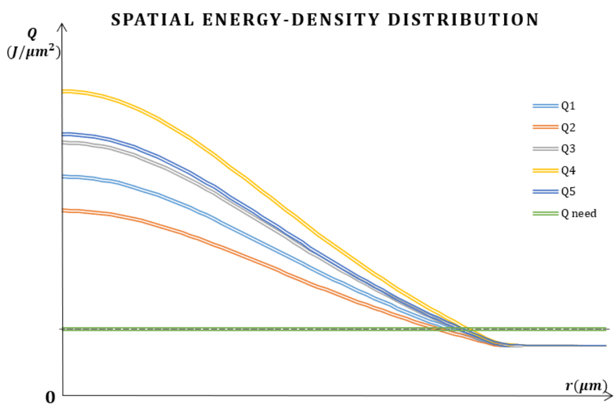


**Fig. 1.** Analysis of energy density variations at the machining site corresponding to different process parameters

Based on the energy-distribution profile, the average laser power, repetition rate, scanning speed, and effective energy accumulation time per unit area are coordinated to determine the appropriate machining time for individual microvias. The processing parameters are then selected to ensure effective ablation of the bilayer Cu-PI structure, which is characteristic of FPC substrates (Fig. 1).

In this study, the machining surface is aligned with the focal plane of the laser beam. The average laser power is reduced to limit excessive peak fluence at the beam center, while the repetition rate and scanning speed are adjusted to control the effective pulse number and pulse overlap within the processing zone. This coordinated adjustment does not simply increase the accumulated fluence; rather, it redistributes the accumulated energy more uniformly and maintains it within the desired processing window. A lower repetition rate increases the temporal interval between successive pulses and allows partial thermal relaxation, whereas a higher galvanometer scanning speed increases the spatial separation between adjacent pulses and suppresses excessive local overlap. As a result, thermal accumulation and surface degradation can be reduced while maintaining sufficient fluence for stable material removal. In regions where the peripheral laser fluence remains below the ablation threshold, a portion of the absorbed energy is dissipated as heat and may contribute to the formation of a heat-affected zone (HAZ); therefore, for a target microvia diameter $D$, the scanning trajectory should be determined based on the effective ablation width, laser spot diameter, and the distribution of accumulated fluence. Under conventional processing conditions, the effective ablation width is limited due to insufficient peripheral fluence and subthreshold energy deposition, and thus a scanning trajectory with a diameter larger than the target feature size is typically required $(D' > D)$ to achieve the desired microvia diameter $D$. By enhancing the effective utilization of absorbed laser energy and suppressing unnecessary thermal accumulation, the proposed method expands the effective ablation region and reduces the required scanning trajectory diameter, thereby decreasing redundant scan length and local pulse overlap, improving thermal damage control, and enabling process time optimization while still ensuring the target microvia diameter is achieved.

## 3. Experimental setup

An industrial laser processing system was used to perform laser microvia machining. The system employed a 355 nm UV Nd:YAG laser as the irradiation source for the experiments. The laser beam was guided through the optical path and focused onto the specimen surface using an F-theta scanning lens. The beam position was controlled by a high dynamic response galvanometer scanner, enabling rapid adjustment of the irradiation position within the machining area and allowing different scanning trajectories to be generated with high precision

To ensure processing stability, the baseline system parameters were established based on the manufacturer's technical specifications. Subsequently, these operational variables were systematically varied to validate the reliability of the proposed evaluation methodology:

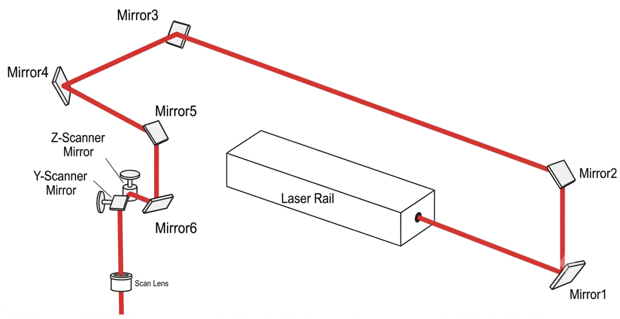


**Fig. 2.** Schematic diagram of the machining system employing a 355 nm UV Nd:YAG laser.

**Table 1.** Processing parameters used in the machining process:

| Parameter | Symbol | Value | Unit |
|---|---|---|---|
| Average Power | $P_{avg}$ | 5-10 | W |
| Pulse Repetition Rate | $f$ | 150-300 | kHz |
| Pulse Width | $\tau$ | 20-25 | ns |
| Wavelength | $\lambda$ | 355 | nm |
| Vacuum Extraction Pressure | $p$ | -13 | kPa |
| Beam Quality Factor | $M^2$ | 1.2 | |
| Scanning Speed | $v$ | 300-800 | mm/s |
| Focal Spot Diameter | $d$ | 20-25 | $\mu$m |

The experimental specimens used in this study were copper-clad laminate (CCL) substrates consisting of a 12$\mu$ m Cu layer and a 20$\mu$ m PI layer. Owing to their ultra-thin and lightweight planar structure, the specimens were mounted on an integrated vacuum chucking fixture during laser processing. The vacuum-assisted clamping system generated a distributed differential pressure through an array of micro-holes on the fixture surface, helping to improve substrate flatness and reduce geometric warping or mechanical distortion during machining [44].

The experimental and machining operations were conducted in an ISO Class 7 cleanroom at an ambient temperature of 25±2°C and atmospheric pressure of 1 atm. The procedure consisted of three main stages. First, the custom-designed fixture was cleaned with 99.5% isopropyl alcohol (IPA) to remove surface contaminants. Second, the CCL substrate was carefully aligned on the fixture and transferred to the laser workstation. Finally, laser machining was performed using predefined kinematic and energy-related parameters, including average laser power, scanning speed, pulse repetition rate, and scanning trajectory. These parameters were selected because pulse fluence, accumulated fluence, pulse spacing, and pulse-to-pulse overlap are key quantities for defining pulsed laser processes and directly affect the accumulated fluence delivered to the local machining region [45]. During machining, a secondary vacuum extraction system was operated to remove ablated copper debris from the ablation zone and substrate surface, thereby reducing particle redeposition and localized machining defects [46].

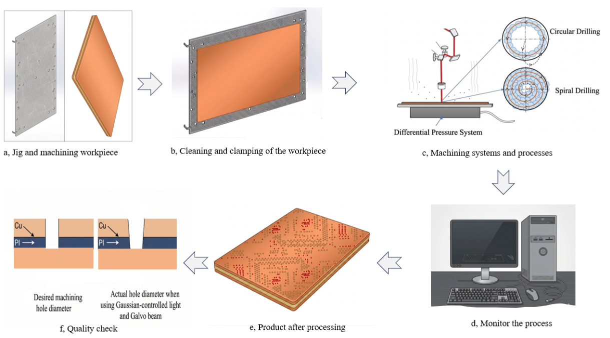


**Fig. 3.** Schematic of the experimental machining process.

Spiral and circular drilling strategies were selected to evaluate the robustness and applicability of the proposed method under scanning trajectories with different energy distribution characteristics and motion patterns [47]. The spiral trajectory produces a continuous variation in scanning radius and pulse overlap, whereas the circular trajectory maintains periodic motion along fixed concentric paths. Comparing these two strategies enables the stability, repeatability, and adaptability of the proposed method to be assessed under different machining conditions.

Scanning electron microscopy (SEM) and laser confocal microscopy were employed as the primary characterization techniques. SEM was used to observe micro scale morphology, sidewall defects, debris adhesion, and recast features, whereas laser confocal microscopy was used to quantitatively measure surface geometry and microvia profiles. In addition, energy dispersive X-ray spectroscopy (EDX) was conducted to examine elemental distribution and compositional variations along the tapered microvia walls [46, 47]. This analysis supports the identification of oxidation, contamination, and resolidified material accumulation, thereby providing evidence for evaluating the surface integrity of microvias after process optimization.

Laser parameters were selected based on the theoretical framework of laser processing, including ablation threshold fluence, absorption coefficient, reflectivity, and safety factors. Accordingly, a feasible parameter window within the allowable operating range of the laser machining system was defined to systematically evaluate the process performance. For the two investigated laser scanning strategies, the corresponding machining parameters are summarized in the table below (Table 2):

To systematically evaluate the effects of parameter adjustment on microvia quality, four processing stages were established with progressively increasing levels of process control for both spiral and circular drilling strategies, as summarized in Table 2. Stage 1 employed the initial parameter set and served as the baseline condition. In Stage 2, the scanning speed was increased while the laser power was reduced at a constant pulse repetition frequency to examine the influence of accumulated energy on material removal and microvia geometry. In Stage 3, the scanning speed was further increased and the pulse repetition frequency was reduced, while the laser power was maintained at the same level as in Stage 2. Relative to the baseline, this stage represented a coordinated adjustment of average laser power, pulse repetition frequency, and scanning speed, allowing the resulting changes in entrance diameter, bottom diameter, and taper ratio to be evaluated. Finally, Stage 4 combined the highest scanning speed with reduced laser power and pulse repetition frequency, together with a vacuum debris extraction system, to assess the overall effects of energy control and debris removal on hole geometry, sidewall quality, and residual material. This staged experimental design enabled the progressive effects of parameter coordination to be monitored and provided a basis for identifying a more suitable processing condition for micro via fabrication.

## 4. result and discussions

### 4.1. Evaluation of microvia taper ratio and dimensional accuracy.

The morphology and overall quality of the machined holes were comprehensively characterized using Scanning Electron Microscopy (SEM), cross-sectional analysis, and laser microscopy. Based on the acquired imaging data, key characteristic parameters were defined to facilitate quantitative evaluation. To ensure statistical reliability, an array of 50 holes was fabricated on each sample under every set of processing conditions.

SEM observations and cross-sectional analysis showed that the machined microvias exhibited tapered rather than perfectly cylindrical profiles. The maximum machining depth occurred near the hole center and gradually decreased toward the sidewalls. This geometrical trend was consistent with the calculated accumulated energy distribution obtained from the proposed model, in which regions receiving higher accumulated energy tended to exhibit greater material removal, whereas regions with lower

**Table 2.** Values of the experimental parameters and the corresponding methods applied during the study:

| Method | Machining stage | Machined Hole Diameter $D(\mu\text{m})$ | Target top diameter $D_{\text{top}}$ $(\mu\text{m})$ | Target minimum bottom diameter $D_{\text{bot}}$ $(\mu\text{m})$ | Scanning Speed $\nu$ (mm/s) | Power $P_{\text{avg}}$ (W) | Frequency $f$(kHz) |
|---|---|---|---|---|---|---|---|
| Spiral Drilling | 1 | 105 | $105 \pm 5.25$ | $89.25 \pm 4.46$ | 446.4 | 8 | 300 |
| | 2 | 105 | 105±5.25 | 89.25±4.46 | 542.4 | 7.5 | 300 |
| | 3 | 105 | $105 \pm 5.25$ | $89.25 \pm 4.46$ | 556.7 | 7.5 | 250 |
| | 4 | 105 | $105 \pm 5.25$ | $89.25 \pm 4.46$ | 700 | 7.0 | 200 |
| Circular Drilling | 1 | 105 | $105 \pm 5.25$ | $89.25 \pm 4.46$ | 446.4 | 8 | 300 |
| | 2 | 105 | $105 \pm 5.25$ | $89.25 \pm 4.46$ | 542.4 | 7.5 | 300 |
| | 3 | 105 | $105 \pm 5.25$ | $89.25 \pm 4.46$ | 556.7 | 7.5 | 250 |
| | 4 | 105 | $105 \pm 5.25$ | $89.25 \pm 4.46$ | 700 | 7.0 | 200 |

**Table 3.** SEM images and cross-sectional views of the machined microvias

| Spiral Drilling | | | |
|---|---|---|---|
| 1 | 2 | 3 | 4 |
| 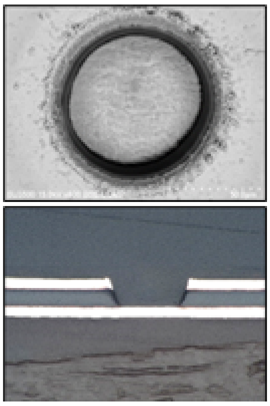 | 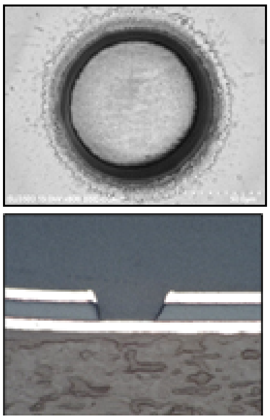 | 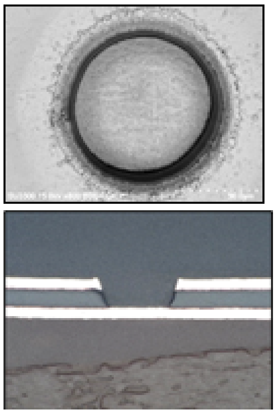 | 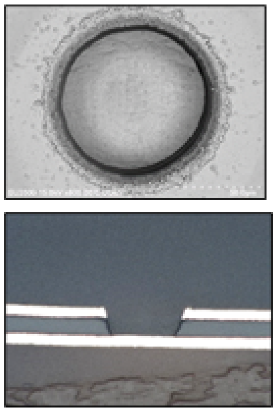 |
| Taper Ratio: 69.04% | Taper Ratio: 67.70% | Taper Ratio: 81.60% | Taper Ratio: 87.98% |
| **Circular Drilling** | | | |
| 1 | 2 | 3 | 4 |
| 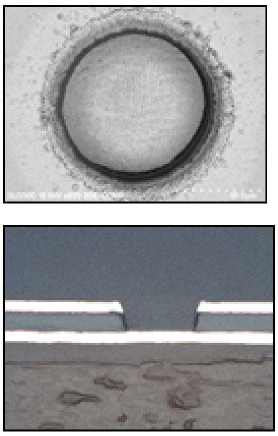 | 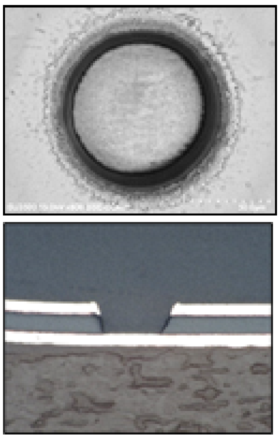 | 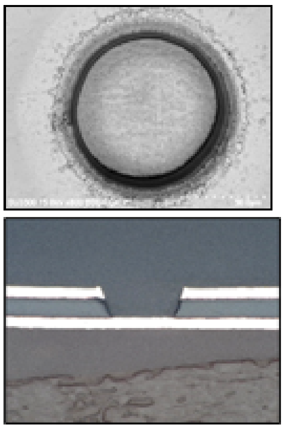 | 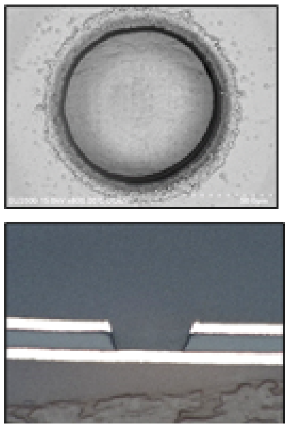 |
| Taper Ratio: 85.16% | Taper Ratio: 82.65% | Taper Ratio: 89.63% | Taper Ratio: 91.58% |

accumulated energy showed reduced machining depth. These observations indicate that the spatial distribution of accumulated energy along the scanning trajectory is closely related to the resulting machining depth and taper of the microvias. Laser microscopy measurements were subsequently used to determine the overall taper ratio of 50 microvias as follows:

$$\text{Taper\_ratio} = 100\% \times \left( \frac{\sum_{i=0}^{50} D_{\text{bot},i}}{\sum_{i=0}^{50} D_{\text{top},i}} \right) \tag{5}$$

Stage 2 produced lower geometrical quality than the baseline condition. The taper ratio decreased from 69.04% to 67.70% for spiral drilling and from 85.16% to 82.65% for circular drilling, corresponding to reductions of 1.34 and

2.51 percentage points, respectively. This deterioration was attributed to the combined effects of reduced laser power and lower pulse overlap caused by the increased scanning speed, resulting in insufficient accumulated energy for uniform material removal. More pronounced thermal deformation and surface defects were also observed under this condition.

In Stage 3, reducing the pulse repetition frequency while maintaining a relatively high scanning speed improved the hole cylindricity and morphological stability. The taper ratio increased to 81.60% for spiral drilling and 89.63% for circular drilling, representing improvements of 12.56 and 4.47 percentage points relative to Stage 1, respectively. Although the lower repetition frequency reduced the number of pulses delivered per unit scanning length, it increased the interval between successive pulses and allowed partial thermal relaxation within the irradiated region. This balance suppressed excessive local heat accumulation and improved the uniformity of material removal. These results indicate that appropriate coordination of scanning speed and pulse repetition frequency can improve microvia quality by controlling pulse accumulation and thermal relaxation.

The best machining performance was achieved in Stage 4, where further parameter coordination was combined with vacuum assisted debris extraction. The combination of high scanning speed, reduced laser power, and reduced pulse repetition frequency limited excessive local energy concentration while maintaining sufficient accumulated fluence for effective material removal. The vacuum extraction system also removed debris generated during machining, thereby reducing material redeposition, secondary heat accumulation, and surface defects. Consequently, the taper ratio reached 87.98% for spiral drilling and 91.58% for circular drilling, corresponding to improvements of 18.94 and 6.42 percentage points relative to Stage 1. The consistent improvements observed for both trajectories demonstrate that the proposed strategy can enhance taper control, surface quality, and process stability. The performance achieved in Stage 4 should therefore be attributed to the combined effects of the laser parameter coordination established in Stage 3 and the additional debris removal provided by the vacuum extraction system.

Geometrical measurements were obtained by laser microscopy from 50 microvias per specimen. The entrance and bottom diameters were compared with the design values and used to calculate the taper ratio. Table 3 presents the taper ratios derived from SEM and cross-sectional analysis, whereas Table 4 summarizes the laser microscopy measurements for Stages 1 and 4 to compare dimensional accuracy, surface quality, and process stability.

**Table 4.** Top and bottom diameter measurement results obtained using the VHX Laser Microscope

| Process | Stage 1 (Bottom - Top) $\mu$m | Stage 4 (Bottom - Top) $\mu$m |
|---|---|---|
| Spiral Drilling | 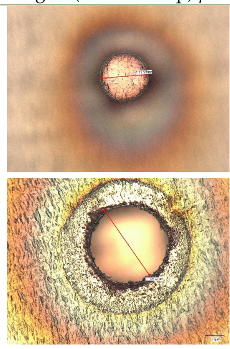 Bot - Top: 73.59-107.42 | 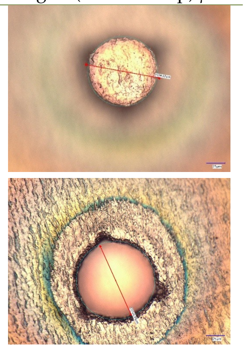 Bot - Top: 94.02-106.35 |
| Circular Drilling | 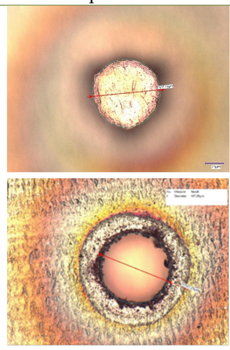 Bot - Top: 73.59-107.42 | 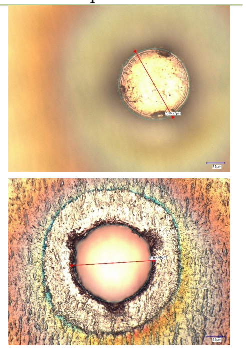 Bot - Top: 94.02-106.35 |

Comparison of the first and fourth machining trials showed clear improvements in microvia dimensions. After process optimization, the bottom diameter increased and both the entrance and bottom diameters approached their target values. The spiral strategy showed a marked reduction in dimensional deviations, while the circular strategy exhibited a similar improvement trend. Overall, both methods achieved better dimensional accuracy, taper control, and geometrical quality.

The diameters of 50 randomly selected microvias on each specimen were measured using laser microscopy and analyzed using geometrical distribution maps and histograms to evaluate dimensional variation and diameter distributions. The results demonstrate that the optimized machining strategy improved dimensional control for both spiral and circular drilling. For spiral drilling, the most pronounced improvement was observed in the bottom diameter, as shown in Fig. 4a. At Stage 1, the mean bottom diameter was only $74.06 \pm 0.16\mu$ m, and none of the measured microvias fell within the specified design tolerance range, corresponding to a compliance rate of 0%. After applying the optimized machining strategy at Stage 4, the mean bottom diameter increased to $93.59 \pm 0.13\mu$ m,

**Table 5.** Comparison of microvia geometry for spiral and circular drilling.

| Drilling strategy stage | Top diameter, Mean ± SD (μm) | Within Top tolerance (%) | Bottom diameter, Mean ± SD (μm) | Within bottom tolerance (%) | Taper ratio (%) |
|---|---|---|---|---|---|
| Spiral stage 1 | 107.26 ± 0.16 | 100 | 74.06 ± 0.16 | 0 | 69.04 |
| Spiral stage 4 | 106.38 ± 0.09 | 100 | 93.59 ± 0.13 | 100 | 87.98 |
| Circular stage 1 | 107.09 ± 0.6 | 100 | 91.2 ± 1.15 | 100 | 85.16 |
| Circular stage 4 | 105 ± 0.70 | 100 | 96.16 ± 0.62 | 100 | 91.58 |

with 100% of the measured microvias falling within the specified tolerance range. The clear shift of the histogram toward the required dimensional range demonstrates a substantial improvement in bottom diameter control. In contrast, the entrance diameter changed only slightly, from $107.26 \pm 0.16\mu$ m at Stage 1 to $106.38 \pm 0.09\mu$ m at Stage 4, with 100% dimensional compliance achieved under both conditions. The lower standard deviation at Stage 4 also indicates a more concentrated entrance diameter distribution after process optimization.

The pronounced improvement in the bottom diameter during spiral drilling may be attributed to the combined effects of the outward to inward scanning trajectory and vacuum assisted debris extraction. During machining, the effective removal of copper debris and ablation products suppresses material redeposition and reduces laser beam shielding by ejected particles. As the scanning trajectory progressively moves toward the central and bottom regions of the microvia, a greater proportion of the incident laser energy can interact effectively with the remaining material, thereby enhancing material removal at the hole bottom and increasing the resulting bottom diameter.

For circular drilling, changes were observed in both the entrance and bottom diameters after application of the optimized machining conditions, as shown in Fig. 4b. The mean entrance diameter decreased from $107.09 \pm 0.60\mu$ m at Stage 1 to $105.00 \pm 0.70\mu$ m at Stage 4, while 100% of the measured microvias remained within the specified entrance diameter tolerance at both stages. This result indicates that circular drilling maintained effective control of the entrance diameter while shifting the mean value closer to the target dimension. The mean bottom diameter increased from $91.20 \pm 1.15\mu$ m at Stage 1 to $96.16 \pm 0.62\mu$ m at Stage 4. According to the dimensional acceptance criteria applied in this study, 100% of the measured microvias satisfied the specified bottom diameter tolerance at both stages. In addition, the standard deviation decreased from 1.15 to $0.62\mu$ m, indicating a narrower bottom diameter distribution and improved dimensional uniformity after optimization.

Overall, the mean values, standard deviations, and histogram distributions reveal different dimensional control characteristics for the two scanning strategies. Spiral drilling produced a particularly pronounced improvement in the bottom diameter, with the dimensional compliance rate increasing from 0% to 100%, whereas circular drilling maintained a high level of dimensional compliance for both the entrance and bottom diameters while reducing the dispersion of the bottom diameter measurements after optimization. Together with the improvement in taper ratio discussed previously, these results demonstrate that the proposed machining strategy not only improves the overall microvia profile but also brings the critical hole dimensions closer to the intended design requirements.

The simultaneous improvements in microvia diameter and taper ratio are of particular practical importance for subsequent copper plating and large scale FPC manufacturing. In particular, a sufficiently large bottom diameter combined with a less constricted microvia profile can provide more favorable geometrical conditions for plating solution access to the deeper regions of the microvia and for subsequent copper deposition along the sidewalls and bottom surface. In mass production, maintaining these geometrical characteristics consistently across a large number of microvias is an important prerequisite for achieving stable and repeatable downstream processing. However, because copper plating was not directly performed or characterized in the present study, the current results cannot be used to quantitatively confirm an improvement in the final plating quality, such as copper thickness, deposition uniformity, or interconnection reliability. Instead, the improved diameter control and taper ratio should be regarded as important geometrical prerequisites that provide more favorable conditions for subsequent metallization and copper plating.

Once the geometrical and dimensional requirements of the microvias have been satisfied, the next critical aspect is the internal surface quality, particularly the presence of carbon containing residues on the microvia walls, which may further influence subsequent metallization quality and interconnection performance.

### 4.2. EDX analysis of elemental composition and microvia quality.

To complement the geometrical and morphological evaluation, EDX analysis was performed to identify elemental

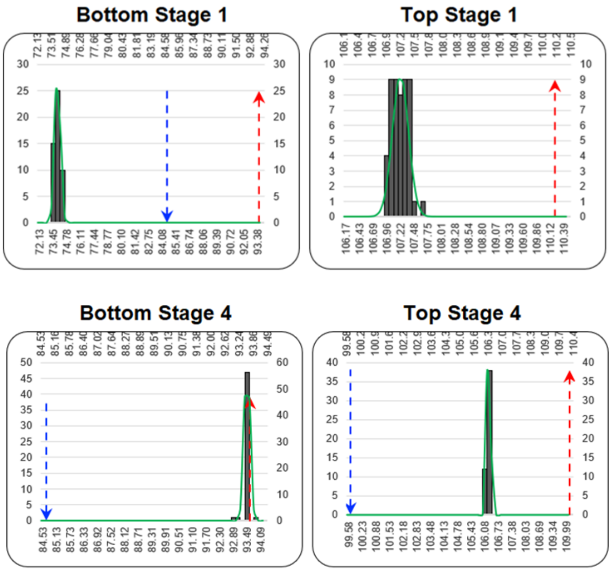


**(a)** Spiral Drilling

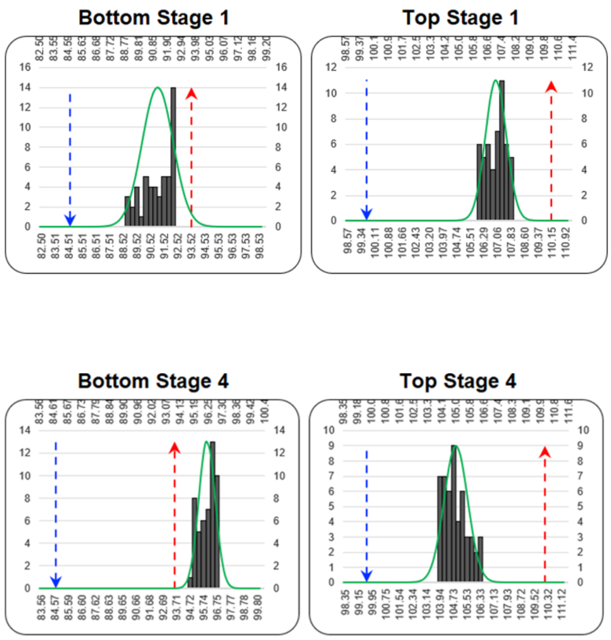


**(b)** Circular Drilling

**Fig. 4.** Spatial distribution and statistical variation of microvia diameters before and after applying the proposed machining strategy.

compositional changes on the microvia walls after machining. For the Cu-PI structure, the Carbon and Cu signals were used to assess carbonization, oxidation, and material redeposition, thereby clarifying the influence of the proposed machining strategy on microvia surface quality.

A total of six microvias were sectioned to prepare cross-sectional samples for evaluating morphological and compositional changes on the hole walls after machining. Among them, three representative microvias, including two located near the corner regions and one located at the central region of the CCL specimen, were selected for image presentation in the manuscript. These cross-sectional images were used to illustrate differences in hole-wall morphology and machining quality between Stage 1 and Stage 4 for each drilling method. The EDX measurement area was fixed near the central region of the hole wall to ensure consistency when comparing carbon content and related elemental signals.

The EDX results show that the carbon content on the microvia wall decreased after applying the proposed machining strategy. For spiral drilling, the average carbon content decreased from 11.87% in Stage 1 to 9.29% in Stage 4, corresponding to a reduction of 2.58 percentage points, or approximately 21.74% relative to the initial value. For circular drilling, the carbon content decreased from 8.86% to 7.54%, corresponding to a reduction of 1.32 percentage points, or approximately 14.90%. Due to the tapered geometry and three-dimensional morphology of the microvias, the EDX results may be influenced by local surface orientation, X-ray shadowing, surface roughness and topography, as well as variations in the effective electron interaction volume and sampling depth. These factors may alter the detected X-ray signal intensity and consequently affect the quantitative accuracy of the elemental analysis. Therefore, the measured elemental concentrations were interpreted primarily in terms of relative trends among different machining conditions under identical analytical settings, rather than as absolute compositional values. For each value reported in Table 6, the measurement uncertainty was evaluated to assess the reliability of the measurement procedure. For the spiral drilling method, the average measurement uncertainty was 9.30% at Stage 1 and decreased to 8.67% at Stage 4. Similarly, for the circular drilling method, the uncertainty decreased from 8.58% at Stage 1 to 7.82% at Stage 4. The relatively small variation in measurement uncertainty between the two stages indicates good measurement stability and repeatability. Furthermore, the reduced measurement uncertainty observed at Stage 4 for both drilling strategies indicates a lower dispersion of the measured data, reflecting improved process stability and thereby enhancing the reliability of the experimental results.

Although the reduction in carbon content was not drastic, these results indicate that the proposed machining strategy did not deteriorate the chemical quality of the microvia walls rather, it contributed to reducing carbon-containing residues after machining. This reduction may be associated with lower localized thermal accumulation and suppressed

**Table 6.** EDX analysis of the residual carbon content in the microvia holes

| Process | Stage | Result Image | Process | Stage | Result Image |
|---|---|---|---|---|---|
| Spiral Drilling | Stage 1 | 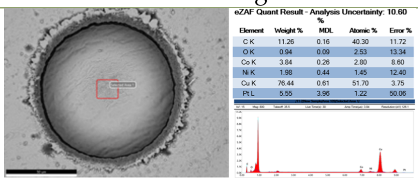 | Circular Drilling | Stage 1 | 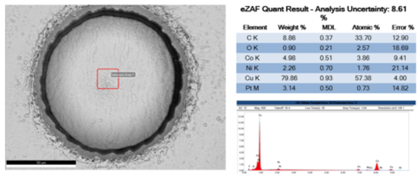 |
| | | 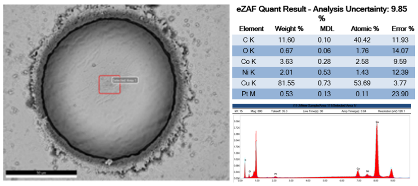 | | | 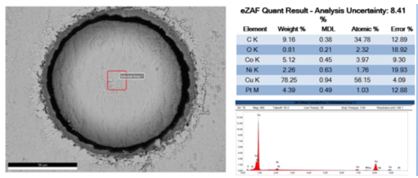 |
| | | 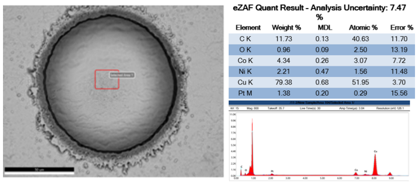 | | | 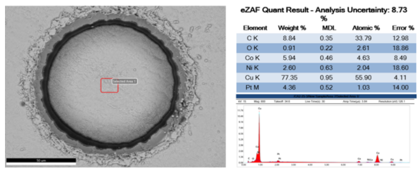 |
| | Stage 4 | 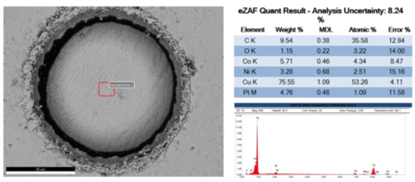 | | Stage 4 | 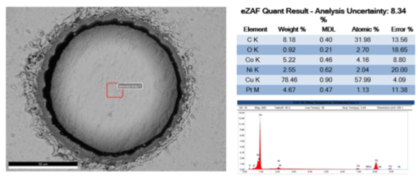 |
| | | 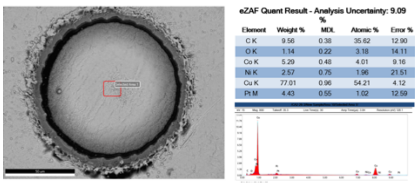 | | | 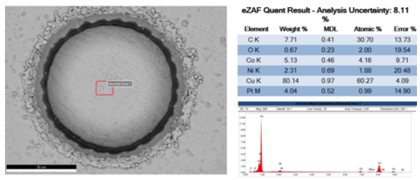 |
| | | 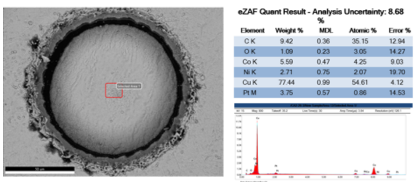 | | | 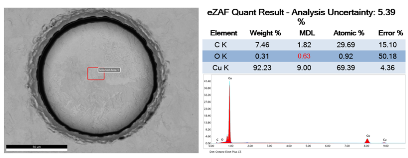 |

thermal decomposition of the PI layer, resulting from the coordinated laser parameters and pressure-assisted debris extraction. In addition, the lower carbon content observed for circular drilling in both Stage 1 and Stage 4 further supports the advantage of circular trajectories in improving surface cleanliness and suppressing carbonization on the microvia walls, consistent with previous studies showing that circular or concentric scanning trajectories can enhance geometrical stability, reduce localized thermal accumulation, and improve the overall quality of laser-drilled holes.

## 5. Conclusions

This study proposes a nanosecond UV laser processing strategy for microvia fabrication in Cu-PI CCL by coordinating average laser power, pulse repetition rate, scanning speed, and vacuum assisted debris extraction. This coordinated approach enables improved control of the accumulated energy distribution, limits localized heat accumulation, and reduces material redeposition on the microvia sidewalls.

Within the investigated range, the proposed strategy improved microvia geometry for both scanning trajectories. The taper ratio increased from 69.04% to 87.98% for spiral drilling and from 85.16% to 91.58% for circular drilling, while the bottom diameter approached the target value. EDX analysis also showed that the sidewall carbon signal decreased from 11.87% to 9.29% and from 8.86% to 7.54%, respectively, supporting a reduction in carbon containing

**Table 7.** Definitions and units of the principal parameters in the accumulated-energy model

| Symbol | Description | Units |
|---|---|---|
| $I_i(t, r)$ | Instantaneous power density of the $i^{\text{th}}$ pulse | $W/\mu m^2$ |
| $Q_i(r)$ | Fluence delivered by a single pulse at position $r$ | $J/\mu m^2$ |
| $Q_{\text{acc}}(r)$ | Cumulative fluence resulting from multiple pulses at position $r$ | $J/\mu m^2$ |
| $Q_{\text{th}}$ | Ablation threshold fluence | $J/\mu m^2$ |
| $P_{\text{avg}}$ | Average laser power | W |
| $f$ | Pulse repetition frequency | kHz |
| $\tau$ | Temporal width parameter of the Gaussian pulse | ns |
| $t$ | Time within an individual pulse | ns |
| d | Laser spot diameter at the workpiece surface | $\mu$m |
| $r$ | Spatial position under consideration | $\mu$m |
| $r_i$ | Center position of the $i^{\text{th}}$ pulse | $\mu$m |
| $i$ | Pulse index | |
| $n_{\text{eff}}$ | Effective number of pulses contributing at the position under consideration. | |
| $D$ | Target microvia diameter | $\mu$m |
| $D'$ | Scanning trajectory diameter | $\mu$m |

residues and improved surface cleanliness.

However, the processing window established in this study has been validated only for the investigated Cu-PI CCL structure and nanosecond UV laser system. Therefore, the present parameter set cannot be directly transferred to other material systems or multilayer structures. Changes in material type, number of layers, stacking sequence, or individual layer thickness alter key properties such as optical absorption, reflectivity, thermal conductivity, ablation threshold, and interfacial bonding strength. Accordingly, the laser wavelength, average power, pulse repetition rate, scanning speed, focal position, scanning diameter, and number of passes must be recalibrated for each specific processing objective.

Nevertheless, the proposed framework, which integrates accumulated energy, Galvo scanning dynamics, and vacuum assisted debris extraction, may be transferable at the methodological level. It may be extended to other multilayer material systems, including metal and polymer structures, PCB substrates, multilayer metals, composites, and semiconductor wafers, provided that the geometric targets, allowable thermal effects, ablation mechanisms, and surface quality requirements are clearly defined.

In addition, circular and spiral trajectories can be programmed directly on existing industrial Galvo systems without substantial equipment modification. Although their relatively long paths may increase laser exposure time, reducing the scanning diameter and increasing the scanning speed can shorten the laser scanning time per microvia. However, overall throughput also depends on the number of passes, positioning time, Galvo acceleration and deceleration, and dwell time. Therefore, the present results are insufficient to confirm an improvement in total production throughput.

Although laser power, pulse repetition rate, and scanning speed were varied during the experiments, the present study primarily focused on elucidating the effects of laser power, pulse repetition rate, and position-dependent accumulated energy distribution on microvia machining quality. The scanning speed was selected from predefined processing conditions and was not incorporated into the proposed mathematical model as an independent variable. Consequently, a unified mathematical model describing the quantitative relationship among laser power, pulse repetition rate, scanning speed, and material removal has not yet been established. Future work will focus on developing such a model and its corresponding analytical framework to quantitatively characterize these coupled effects, thereby providing a theoretical basis for predictive process optimization and intelligent parameter selection in industrial laser microvia drilling.

## Acknowledgements

This research is funded by Hanoi University of Science and Technology (HUST) under project number T2024-TĐ-028.

The authors would like to express their sincere gratitude to the Precision Engineering & Smart Measurement Laboratory and Sumitomo Corporation for their support throughout the experimental phase of this research.

## Appendix

Table 7

## References


**[1]** L. Zheng, S. Lin, H. Lu, B. Huang, Y. Liu, J. Wang, X. Wei, J. Wang, and C. Wang, (2024) *"Characterization of Micro-Holes Drilled Using a UV Femtosecond Laser in Modified Polyimide Flexible Circuit Boards"* **Micromachines** ***15***(9): 1078. DOI: 10.3390/mi15091078.

**[2]** H. Lu, Z. Ou, B. Huang, X. Huang, C. Wang, and L. Zheng, (2022) *"Study on Micro-holes Processing of High Frequency Flexible Copper Clad Laminate Substrate via Femtosecond Laser"* **Mechanical Science and Technology for Aerospace Engineering** ***41***(8): 1224–1230. DOI: 10.13433/j.cnki.1003-8728.20220151.

**[3]** K.-R. Kim, J.-H. Cho, N.-Y. Lee, H.-J. Kim, S.-H. Cho, H.-J. Park, and B. Choi, (2016) *"High-precision and ultrafast UV laser system for next-generation flexible PCB drilling"* **Journal of Manufacturing Systems** ***38***: 107–113. DOI: 10.1016/j.jmsy.2015.12.001.

**[4]** H. Zheng, E. Gan, and G. C. Lim, (2001) *"Investigation of laser via formation technology for the manufacturing of high density substrates"* **Optics and Lasers in Engineering** ***36***(4): 355–371. DOI: 10.1016/S0143-8166(01)00057-4.

**[5]** Z. Huang, Y. Cai, Z. Zhang, N. Li, F. Shi, W. Lin, and H. Liu, (2025) *"Laser drilling of micro-holes with controllable taper using 355 nm nanosecond laser"* **Optics & Laser Technology** ***181***: 111929. DOI: 10.1016/j.optlastec.2024.111929.

**[6]** K. C. Yung, D. W. Zeng, and T. M. Yue, (2002) *"High repetition rate effect on the chemical characteristics and composition of Upilex-S polyimide ablated by a UV Nd:YAG laser"* **Surface and Coatings Technology** ***160***(1): 1–6. DOI: 10.1016/S0257-8972(02)00384-5.

**[7]** P. Deepu, T. Jagadesh, and M. Duraiselvam, (2023) *"Investigations into morphology and surface integrity of micro-hole during femtosecond laser drilling of titanium alloy"* **Journal of the Brazilian Society of Mechanical Sciences and Engineering** ***45***(10): 516. DOI: 10.1007/s40430-023-04449-7.

**[8]** Y. Dong, Q. Ye, Q. Li, X. Guo, S. Zhang, and N. Hou, (2022) *"Numerical Simulation and Validation of Multiscale 3D Laser Spiral Machining of Microholes"* **Laser and Particle Beams** ***2022***: e22. DOI: 10.1155/2022/2455226.

**[9]** M. Li, Y. Chen, L. Dong, D. Liu, and X. Sun, (2025) *"Quality Evaluation of Micro-Holes Processed by Efficient One-Step Femtosecond Laser Helical Drilling Method in Nickel-Based Superalloy"* **Applied Sciences** ***15***(8): 4384. DOI: 10.3390/app15084384.

**[10]** Z. Gu, Y. He, J. Yang, Y. Fu, J. Ji, Y. Zhang, J. Li, and G. Liu, (2023) *"Dual-path micro-holes process for 0Cr17Ni7Al stainless steel thin plate with picosecond laser"* **Journal of Manufacturing Processes** ***101***: 1224–1233. DOI: 10.1016/j.jmapro.2023.07.004.

**[11]** Z. Qin, J. Yang, J. Niu, L. Chen, K. Cao, T. Jia, and H. Xu, (2025) *"Precision control of hole morphology by modulating femtosecond laser beam track with a four-wedge drilling system"* **Optics & Laser Technology** ***192***: 113972. DOI: 10.1016/j.optlastec.2025.113972.

**[12]** X. Sun, X. Dong, K. Wang, P. Fan, T. Sun, X. Mei, and Z. Fan, (2024) *"Femtosecond laser processing of controlled tapered micro-holes based on dynamic control of relative attitude"* **Optics & Laser Technology** ***170***: 110201. DOI: 10.1016/j.optlastec.2023.110201.

**[13]** S. Gonumakulapalle Lodi and S. Kumar. "Experimental Investigation on the Annular Drilling of Acute Angle Micro-Holes in Nickel Based Superalloy With Femtosecond Laser". In: *Proceedings of the ASME 2024 International Mechanical Engineering Congress and Exposition (IMECE2024), Volume 2: Advanced Manufacturing* (Portland, Oregon, USA, Nov. 17–21, 2024). Paper No. IMECE2024-145332, 7 pages. 2024, V002T03A068. DOI: 10.1115/IMECE2024-145332.

**[14]** X. Liu, Y. Wang, Y. Yang, L. Bao, Y. Liu, W. Zhang, and L. Li, (2025) *"Fabrication of micro holes with high surface quality and integrity by high-speed laser trepanning and electrochemical post-treatment"* **The International Journal of Advanced Manufacturing Technology** ***137***: 67–81. DOI: 10.1007/s00170-025-15229-z.

**[15]** N. Zhang, M. Wang, M. Ban, L. Guo, and W. Liu, (2024) *"Femtosecond laser drilling 100 μm diameter micro holes with aspect ratios >20 in a nickel-based superalloy"* **Journal of Materials Research and Technology** ***28***: 1415–1422. DOI: 10.1016/j.jmrt.2023.12.049.

**[16]** P. Deepu and T. Jagadesh, (2024) *"Femtosecond Laser Micro Drilling of Cooling Holes on Thermal Barrier Coated Titanium Alloy for Aeroengine Application"* **Journal of Materials Engineering and Performance** ***33***(19): 10242–10263. DOI: 10.1007/s11665-023-08679-7.

**[17]** Z. Zhao, Y. Yu, R. Sun, W. Zhao, H. Guo, Z. Zhang, and C. Wang, (2023) *"Design of a Femtosecond Laser Percussion Drilling Process for Ni-Based Superalloys Based on Machine Learning and the Genetic Algorithm"* **Micromachines** ***14***(11): 2110. DOI: 10.3390/mi14112110.

**[18]** L. Wang, Y. Rong, L. Xu, C. Wu, and K. Xia, (2025) *"Study on Laser Drilling of Micro-Holes Using a Breakthrough Detection Method"* **Materials** ***18***(16): 3764. DOI: 10.3390/ma18163764.

**[19]** B. S. Shin, J. Y. Oh, and H. Sohn, (2007) *"Theoretical and experimental investigations into laser ablation of polyimide and copper films with 355-nm Nd:YVO$_4$ laser"* **Journal of Materials Processing Technology** ***187–188***: 260–263. DOI: 10.1016/j.jmatprotec.2006.11.106.

**[20]** T. Karkantonis, E. Pelletier, D. Grant, and D. Karnakis, (2024) *"Femtosecond Laser Drilling of High-Density Micro-Holes on Metals Using MHz Burst Mode"* **Journal of Laser Micro/Nanoengineering** ***19***(3): 241–246. DOI: 10.2961/jlmn.2024.03.2011.

**[21]** C. Zhang, M. Li, B. Ye, J. Wu, Z. Wang, and X. Li, (2022) *"Electrons dynamics control micro-hole drilling using temporally/spatially shaped femtosecond laser"* **Opto-Electronic Engineering** ***49***(2): 210389. DOI: 10.12086/oee.2022.210389.

**[22]** Y. Ding, C. Wang, Z. Gao, X. Jiang, S. Wang, X. Jia, L. Liu, and J. Duan, (2025) *"Rapid Fabrication of Large-Area Anti-Reflective Microholes Using MHz Burst Mode Femtosecond Laser Bessel Beams"* **Nanomaterials** ***15***(22): 1726. DOI: 10.3390/nano15221726.

**[23]** N. Ren, J. Zhang, Z. Li, D. Qi, H. Zhang, and K. Xia, (2025) *"The Effects of Static- and Flowing-Water-Assisted Methods on the Quality of Femtosecond Laser Drilling of Thermal-Barrier-Coated Superalloys"* **Metals** ***15***(3): 261. DOI: 10.3390/met15030261.

**[24]** R. Zhang, H. Zhang, R. Ke, and X. Wang, (2025) *"Fabrication of high aspect ratio and low taper angle microholes utilizing complex water-assisted femtosecond laser drilling"* **Optics & Laser Technology** ***185***: 112608. DOI: 10.1016/j.optlastec.2025.112608.

**[25]** X. Jiang, X. Xu, H. Zhou, C. Wang, X. Jia, Y. Ding, Z. Gao, S. Wang, L. Liu, and J. Duan, (2025) *"Femtosecond laser burst mode combined with wet etching for fabricating surface microholes on sapphire"* **Applied Physics A** ***131***: 888. DOI: 10.1007/s00339-025-09029-1.

**[26]** K. Xia, Z. Li, D. Qi, J. Di, H. Wang, H. Lin, and N. Ren, (2026) *"Influence of dynamic water-assisted method on the quality of femtosecond laser spiral drilling in thermal barrier coated superalloys"* **Optics & Laser Technology** ***194***: 114377. DOI: 10.1016/j.optlastec.2025.114377.

**[27]** M. Mendiratta and S. Prakash, (2025) *"Investigation and process optimization of backside thin water layer assisted laser micro-drilling of titanium"* **Lasers in Manufacturing and Materials Processing** ***12***(2): 318–345. DOI: 10.1007/s40516-025-00288-7.

**[28]** Y. Liu, P. Ouyang, Z. Zhang, W. Xue, Y. Wang, H. Zhu, K. Xu, J. Wang, J. Cai, and J. Lu, (2025) *"Multi-energy field simulation and experimental research on backside water assisted laser processing for thin-walled irregular metal micro-holes"* **Optics & Laser Technology** ***187***: 112790. DOI: 10.1016/j.optlastec.2025.112790.

**[29]** N. Ren, S. Yao, Z. Wu, Y. Zheng, J. Di, L. Wang, and K. Xia, (2025) *"The influence of different water-assisted methods on femtosecond laser layered-ring trepanning in silicon nitride ceramics"* **Optics & Laser Technology** ***185***: 112605. DOI: 10.1016/j.optlastec.2025.112605.

**[30]** Y. Tao, Z. Wang, S. Hu, Y. Feng, F. Yang, and G. Li, (2024) *"Improving the quality of laser drilling by assisted process methods of static solution and mist blowing"* **Micromachines** ***15***(4): 515. DOI: 10.3390/mi15040515.

**[31]** A. Riveiro, F. Quintero, F. Lusquiños, J. Del Val, R. Comesaña, M. Boutinguiza, and J. Pou, (2012) *"Experimental study on the CO$_2$ laser cutting of carbon fiber reinforced plastic composite"* **Composites Part A: Applied Science and Manufacturing** ***43***(8): 1400–1409. DOI: 10.1016/j.compositesa.2012.02.012.

**[32]** L. Tunna, A. Kearns, W. O'Neill, and C. J. Sutcliffe, (2001) *"Micromachining of copper using Nd:YAG laser radiation at 1064, 532, and 355 nm wavelengths"* **Optics & Laser Technology** ***33***(3): 135–143. DOI: 10.1016/S0030-3992(00)00126-2.

**[33]** W. Zhang, Y. L. Yao, and K. Chen, (2001) *"Modelling and analysis of UV laser micromachining of copper"* **The International Journal of Advanced Manufacturing Technology** ***18***(5): 323–331. DOI: 10.1007/s001700170056.

**[34]** T.-H. Chen, R. Fardel, and C. B. Arnold, (2018) *"Ultrafast z-scanning for high-efficiency laser micro-machining"* **Light: Science & Applications** ***7***: 17181. DOI: 10.1038/lsa.2017.181.

**[35]** P. I. Szabó, D. Ugi, B. Gilicze, Z. Dankházi, S. Lipcsei, Z. Homik, and Z. Tóth, (2023) *"Micromachining using the high energy flat-top beam of a femtosecond pulse UV laser system: micropillar prefabrication"* **Applied Physics A** ***129***(6): 403. DOI: 10.1007/s00339-023-06679-x.

**[36]** I. Miraoui, M. Zaied, and M. Boujelbene, (2014) *"Effect of Laser Beam Diameter on Cut Edge of Steel Plates Obtained by Laser Machining"* **Applied Mechanics and Materials *467***: 227–232. DOI: 10.4028/www.scientific.net/AMM.467.227.

**[37]** X.-H. Nguyen, C.-M. Chen, H.-T. Le, and H.-Y. Lee, (2022) *"Enhancement of a Single-Axis Femtosecond Laser Scanning System by Using Two Galvanometers to Improve the Tele-centricity and the Effective Scanning Length on Laser Process"* **Applied Sciences *12***(23): 12434. DOI: 10.3390/app122312434.

**[38]** D. Franz, T. Häfner, T. Kunz, G. L. Roth, S. Rung, C. Esen, and R. Hellmann, (2022) *"Characterization of a hybrid scanning system comprising acousto-optical deflectors and galvanometer scanners"* **Applied Physics B *128***: 55. DOI: 10.1007/s00340-022-07782-2.

**[39]** M. Garcia-Lechuga and D. Grojo, (2021) *"Simple and robust method for determination of laser fluence thresholds for material modifications: an extension of Liu's approach to imperfect beams"* **Open Research Europe *1***: 7. DOI: 10.12688/openreseurope.13073.2.

**[40]** L. Wang, H. Yang, N. Ren, Z. Wu, and K. Xia, (2022) *"Experimental Characterization of Laser Trepanned Microholes in Superalloy GH4220 with Water-Based Assistance"* **Micromachines *13***(12): 2249. DOI: 10.3390/mi13122249.

**[41]** A. Anjum and A. A. Shaikh, (2023) *"Experimental and analytical modeling for channel profile using $CO_2$ laser considering Gaussian beam distribution"* **Journal of Engineering Research *11***(2): 100035. DOI: 10.1016/j.jer.2023.100035.

**[42]** A. Feuer, R. Weber, R. Feuer, D. Brinkmeier, and T. Graf, (2021) *"High-quality percussion drilling with ultrashort laser pulses"* **Applied Physics A *127***(9): 665. DOI: 10.1007/s00339-021-04818-w.

**[43]** R. Weber, T. Graf, C. Freitag, A. Feuer, T. Kononenko, and V. I. Konov, (2017) *"Processing constraints resulting from heat accumulation during pulsed and repetitive laser materials processing"* **Optics Express *25***(4): 3966–3979. DOI: 10.1364/OE.25.003966.

**[44]** K.-i. Nomura, H. Ushijima, K. Noguchi, N. Miyaguchi, T. Kobayashi, and M. Kawabe, (2016) *"Vacuum chucking assist sheet for fixing flexible sheets during the printing process"* **Microsystem Technologies *22***(12): 2931–2937. DOI: 10.1007/s00542-015-2803-1.

**[45]** T. Fox and F. Mücklich, (2023) *"Development and validation of a calculation routine for the precise determination of pulse overlap and accumulated fluence in pulsed laser surface treatment"* **Advanced Engineering Materials *25***(3): 2201021. DOI: 10.1002/adem.202201021.

**[46]** F. Li, G. Feng, X. Yang, X. Li, G. Ma, and C. Lu, (2020) *"Research on Microhole Processing Technology Based on the Femtosecond-Laser Spiral Trepanning Method"* **Applied Sciences *10***(21): 7508. DOI: 10.3390/app10217508.

**[47]** L. Wang, Y. Rong, L. Xu, C. Wu, and K. Xia, (2025) *"Process Optimization on Trepanning Drilling in Titanium Alloy Using a Picosecond Laser via an Orthogonal Experiment"* **Micromachines *16***(8): 846. DOI: 10.3390/mi16080846.